

# Finite-Size and Gravity Effects on the Thermal Conductivity of $^4\text{He}$ near $T_\lambda$

Guenter Ahlers

*Department of Physics and Center for Nonlinear Science,  
University of California, Santa Barbara, California 93106*

---

## Abstract

This paper reviews the opportunities for microgravity and ground-based measurements of the thermal conductivity  $\lambda(t, L)$  near the bulk superfluid-transition line  $T_\lambda(P)$  of  $^4\text{He}$  confined in cylindrical geometries with axial heat flow. It provides an evaluation of existing data near  $T_\lambda$  at saturated vapor pressure (SVP) in cylinders of  $L = 1\mu\text{m}$  radius, and uses these to derive a scaling function for the resistivity  $R(t, L) = 1/\lambda(t, L)$ . The purpose of future measurements over a wide range of  $L$  and of the pressure  $P$  will be to test the applicability of this function. In the present paper the scaling function is used to predict the conductivity for other values of  $L$  and  $P$ . These predictions are used to assess quantitatively the effect of gravity on potential Earth-based measurements. It is found that the gravity effect for  $R$  is particularly severe below  $T_\lambda$ . The estimate of the gravity effect provides the foundation for the choice of parameters of the proposed microgravity experiment BEST. For typical three mm high samples at SVP, values of  $L$  significantly larger than  $8\mu\text{m}$  can only be investigated fully in micro-gravity. At higher pressures the gravity effect is larger. At 30 bar, samples with  $L > 4\mu\text{m}$  require micro-gravity below  $T_\lambda(P)$ . Modern thermometry has sufficient resolution to permit quantitative measurements of the finite-size effect for values of  $L$  as large as  $100\mu\text{m}$ .

---

## 1 Introduction

An interesting issue in condensed-matter physics is the nature of the interface between solids and fluids. The microscopic aspects of systems near boundaries are difficult to study. However, when the fluid is near a critical point, the boundary layer adjacent to the solid surface acquires a macroscopic thickness. When the fluid phase is of limited spatial extent, the boundary will influence significantly the average macroscopic properties of the system. Thus, a critical fluid system which is confined can be used to study boundary effects. In

addition to these “surface” effects, a system confined in a finite geometry will also exhibit “bulk” finite-size effects; both contributions are expected to be describable within the general context of finite-size scaling[1] and by specific calculations based on the renormalization-group theory (RGT) [2], and we will collectively refer to them as “finite-size effects”.

There is a long history of experimental work on finite-size effects on *equilibrium* properties near  $T_\lambda$ . However, so far all of this work has been restricted to saturated vapor pressure (SVP). A comprehensive review was written recently by Gasparini and Rhee [3]. Much of the older work was carried out in poorly defined geometries with a significant distribution of characteristic sizes such as is found in packed powders, making it difficult to interpret the results quantitatively in terms of modern theories. More recently measurements have been made in more uniform geometries of better known dimensions [4–8]. The interpretations of these results are in part in conflict with theoretical predictions based on scaling arguments [1] and RGT considerations [2]. Thus there is a strong need for additional accurate measurements over a wide range of the pressure  $P$  and of the size  $L$  for precisely known and uniform geometries. Systems with confinement in one, two, and three dimensions, corresponding to parallel-plate, cylindrical, or cubic geometries respectively, are expected to represent three different universality classes and need to be investigated experimentally. The recent microgravity experiment CHeX [9] was a major step towards satisfying the need for more data at SVP for the parallel-plate geometry.

Experiments on *transport* properties in manifestly finite geometries are almost non-existent. Here at least three cases can realistically be investigated. In a parallel-plate geometry one could have the heat flow  $\vec{Q}$  parallel or orthogonal to the plates. In a cylindrical geometry  $\vec{Q}$  most likely would be in the axial direction. Qualitatively different finite-size effects would be expected for the three cases. The most relevant measurements we know of [10] are the ones of the thermal conductivity  $\lambda$  carried out by Kahn and Ahlers [11] (KA) on  $^4\text{He}$  at SVP. Their sample was contained in the long, narrow tubes of a glass capillary array (GCA) (also known as micro-channel plates) [12] and thus represents the cylindrical geometry with axial heat flow. The tube radius  $L$  was  $1\ \mu\text{m}$ . The major goal of the flight-definition project “**B**oundary **E**ffects on transport properties and dynamic finite-size scaling near the **S**uperfluid **T**ransition line of  $^4\text{He}$ ” (**BEST**) is to provide data for  $\lambda$  in the same geometry over a wide range of  $L$  and  $P$ . Plans for this work will build upon the KA measurements and the assumption of finite-size scaling. The present paper describes the *expected* behavior of the system if it is *assumed* that finite-size scaling is valid for the conductivity. The major objective of the experiments will of course be to test this assumption. The predicted scaling function is used to obtain a quantitative assessment of the gravity effect on Earth-based measurements for different  $L$  and typical sample thickness (height)  $h$  and to

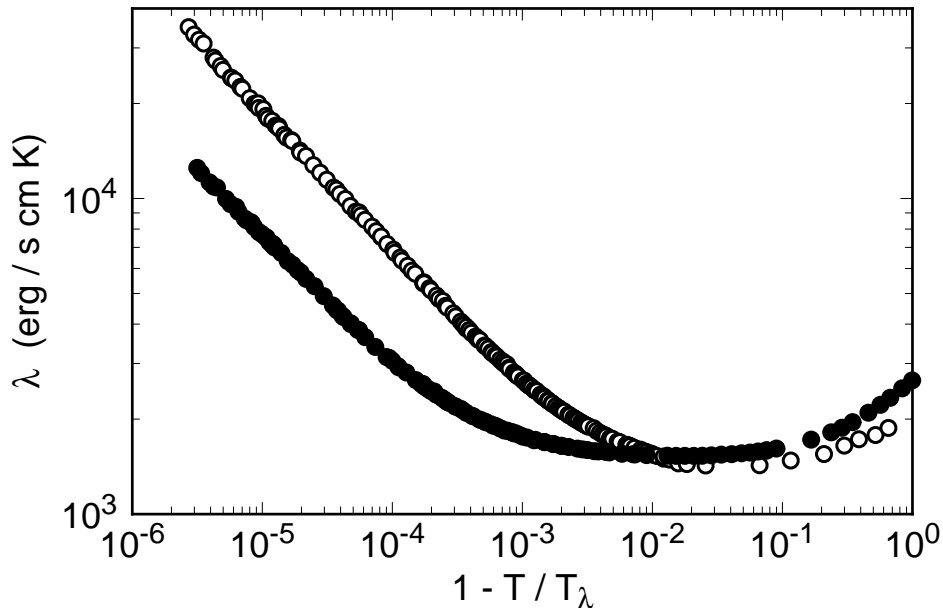


Fig. 1. The thermal conductivity of  ${}^4\text{He}$  above  $T_\lambda$  as a function of the reduced temperature [16] at vapor pressure (open symbols) and at 28 bar (solid symbols). The results are shown on logarithmic scales.

define optimal parameters of the proposed microgravity experiment.

The KA results showed that the thermal resistivity  $R = 1/\lambda$  in the cylindrical geometry remains finite at  $T_\lambda$ , and decays exponentially as the temperature  $T$  is reduced below  $T_\lambda$ . The data confirm that there is no phase transition in the one-dimensional system, as had been expected on general theoretical grounds. Important as these results may be, by themselves they are not adequate to test the ideas of finite-size scaling for transport properties because the dependence upon the characteristic size  $L$  of the geometry is at issue and measurements over a wide range of  $L$  are required. They also do not explore the expected universality of the corresponding scaling function along the  $\lambda$ -line as a function of pressure. Thus the significance of the  $1\ \mu\text{m}$  data would be enormously enhanced by equivalent results for different characteristic sizes and over a range of  $P$ . It turns out that a significant range of  $L$  can be explored only by extending it to relatively large values. However, for  $L \gtrsim 8\ \mu\text{m}$  the effect of Earth's gravity[13] prevents definitive measurements and experiments are feasible only in microgravity.

A quantitative analysis of the conductivity  $\lambda(t, L)$  of the finite system requires a quantitative knowledge of  $\lambda(t) \equiv \lambda(t, \infty)$  for the bulk system. The dependence upon  $t$  of the bulk conductivity, although complicated, is already remarkably well understood both experimentally[14–18] and theoretically[19]. There do remain some unresolved issues, however, which are of interest for their own sake as well as important to the quantitative interpretation of  $\lambda(t, L)$ .

In Fig. 1 we show  $\lambda$  vs.  $t \equiv T/T_\lambda - 1$  on logarithmic scales for saturated vapor pressure (SVP) and for  $P = 28$  bar. Similar results exist at several intermediate pressures, but are omitted here for clarity. For sufficiently small  $t$ , the data to a good approximation fall on straight lines, and thus can be described by the powerlaw

$$\lambda = \lambda_0 t^{-x} . \quad (1)$$

However, on closer inspection one finds that the exponent

$$x \equiv -d[\ln(\lambda)]/d[\ln(t)] \quad (2)$$

is an effective exponent which depends very slightly upon  $t$ . Furthermore, on theoretical grounds one would have expected  $x$  to have a universal asymptotic value equal or close to  $\nu/2$ , which on the basis of second-sound-velocity measurements [20] has a value near 0.3352. However, measurements of  $\lambda$  give a slightly pressure dependent effective value which varies from  $x \simeq 0.44$  at SVP to  $x \simeq 0.41$  at 28 bar. This was explained quantitatively nearly two decades ago[19] by detailed RGT calculations of non-universal (i.e. pressure dependent) non-asymptotic contributions to  $\lambda$ . The quantitative explanation of the rather complicated behavior of  $\lambda(t, P)$  along the entire transition line  $T_\lambda(P)$  is a major success of the RGT. However, the comparison between experiment and theory still has its limitations, as can be seen from the range of the data in Fig. 1. The data are only for  $t \gtrsim 3 \times 10^{-6}$ . For transport properties this is a more severe limitation than for equivalent results for equilibrium properties because the critical region where approximate powerlaw dependence is found is much more narrow. As seen in Fig. 1, at SVP this region is  $t \lesssim 10^{-3}$ . The range becomes even more narrow at higher pressure, being confined to  $t \lesssim 10^{-4}$  at 28 bar. Thus it would be extremely useful to extend the range to smaller  $t$  by several decades to provide a more stringent test of the theory. Some extension of the range can actually be obtained on Earth with the use of high-resolution thermometry[21,22]; but for  $t \lesssim 10^{-7}$  gravity would prevent measurements from being made. [13] In a microgravity environment, this range could be extended by another decade or two. This is particularly important because recent high-resolution measurements[23] at vapor pressure have suggested a departure from the RGT prediction for  $t \lesssim 10^{-6}$ . It is also important for the unambiguous determination of the finite-size contribution for the large values  $L = 25$  or  $50\mu\text{m}$  envisioned for the microgravity experiment. Thus a secondary objective of **BEST** will be to obtain high-quality data of the bulk conductivity along several isobars for  $t \gtrsim 10^{-8}$  or so.

## 2 Theoretical Predictions

At present, the RGT is not sufficiently advanced to provide predictions of the critical behavior of transport properties in a confined geometry near  $T_\lambda$  of  ${}^4\text{He}$ . [24] Thus we can describe the anticipated results only within the general context of phenomenological scaling arguments. Although scaling has been used for finite-size effects on static properties, there is at present *no* experimental foundation for its application to transport properties. Thus our work will provide the first test of finite-size scaling for the dynamics. To formulate the problem more precisely, we assume that  $\lambda(t)$  can be written in the form of Eq. 1. This approximation is justified to the extent to which the data close to  $T_\lambda$  in Fig. 1 fall on straight lines. For the finite system we will find it more convenient to discuss the thermal resistivity  $R(t, L) = 1/\lambda(t, L)$  because the difference between it and  $R(t) \equiv R(t, \infty)$  remains finite. For the cylindrical geometries which we have in mind, we will simply take  $L$  to be equal to the cylinder radius. In that case the finite-size effect well above  $T_\lambda$ , where surface effects dominate, should on geometrical grounds be the same as for parallel plates with spacing  $L$  and with  $\vec{Q}$  parallel to the plates because the ratio of the surface area to the cross sectional area is the same. However, near and below  $T_\lambda$  qualitatively different behavior would be expected for the two cases. Regardless of the geometry, and in analogy to static scaling arguments, we expect the relationship between  $R(t, L)$  and  $R(t)$  to be given by a function only of  $L/\xi$ , where

$$\xi = \xi_0 t^{-\nu} \quad (3)$$

with  $\nu = 0.6705$  [20] is the bulk correlation length above  $T_\lambda$ . Thus we write  $R(t)$  in terms of  $\xi(t)$  as

$$R(t) = R_0 \xi_0^{x/\nu} \xi^{-x/\nu} \quad (4)$$

and make the Ansatz

$$R(t, L) = R(t) \tilde{F}(L/\xi) \quad (5)$$

This appears reasonable above  $T_\lambda$ , but below the transition where  $R(t) = 0$  it is not obvious that this will lead to a meaningful expression. Proceeding nonetheless, we find after some rearrangement the scaling function

$$F(X) = (L/\xi_0)^{x/\nu} [R(t, L)/R_0] \quad (6)$$

with

$$X \equiv (L/\xi_0)^{1/\nu}|t| . \quad (7)$$

Equivalently, one can obtain

$$G(X) = (L/\xi_0)^{x/\nu}[R(t, L) - R(t)]/R_0 . \quad (8)$$

Above  $T_\lambda$  the function  $G(X)$  is more sensitive to the finite-size effect since the bulk resistivity is subtracted; but below the bulk transition  $R(t) = 0$  and thus  $G(X)$  is the same as  $F(X)$ .

The most appealing result would be to find that the functions  $F(X)$  and  $G(X)$  are universal, implying that (for a given geometry) they do not depend on  $L$  and  $P$ . We believe that this universality is particularly uncertain below  $T_\lambda$  where  $R(t) \equiv 0$ . Our concern is enhanced by the fact that (at least for the cylindrical geometry)  $R(t, L) - R(t)$  has a very different dependence upon  $t$  above and below  $T_\lambda$ , as we will see in detail below. Well above the transition, where the difference is expected to be determined by surface effects, experiment suggests that it varies as  $t^{-\nu}$ . However, below  $T_\lambda$  the difference decays *exponentially* as  $|t|$  increases. This behavior suggests that the physical phenomena which dominate the finite-size effects on the two sides of the transition are quite different from each other. The exponential dependence below  $T_\lambda$  suggests that the physics of the superfluid phase comes into play in a crucial way, perhaps in the form of phase-slip phenomena such as in one-dimensional superconductors. Of course this does not exclude the possibility that the finite-size effects on both sides scale with  $\xi$ , and that the functions  $F$  and  $G$  which we have defined are nonetheless universal. Clearly an experimental determination of  $F$  and  $G$  at *several* values of  $L$  and  $P$  will be extremely instructive.

It is to be expected that the functions  $F(X)$  and  $G(X)$  as defined by Eqs. 6 to 8 will be found to be pressure dependent, and thus apparently non-universal. This is so because the simple powerlaw description which we have assumed for  $R(t)$ , although it fits the data extremely well, is inconsistent with universality because the effective exponent  $x$  depends on  $P$  as discussed in Sect. 4.1 below. A more complete theory, based on a universal asymptotic  $R(t)$  and the known non-universal non-asymptotic corrections, might recover the expected universality as a function of pressure. However, such a theory does not appear to exist at this time. Thus we are at present unable to make quantitative predictions of the pressure dependence of the finite-size effect. However, we feel that the determination at SVP of the function  $G(X)$  for the *excess* resistivity should still be valid to a reasonable approximation even at the higher pressures and that it should provide a reasonable guide for the design of new

experiments when it is used with the pressure dependent  $R_0$ ,  $\xi_0$ , and  $x$ .

### 3 Need for Micro-Gravity

The main purpose of the planned work is to determine whether  $R(t, L)$  for the cylindrical geometry can indeed be written in the form of Eqs. 6 and 8, and to determine whether the functions  $F(X)$  and  $G(X)$  are universal, *i.e.* independent of  $L$  and  $P$ . This will be possible only when data become available along several isobars over a significant range of  $L$  and of  $t$ . There are several factors which restrict the range of  $L$  which can be used. One of them is the practical issue of the availability of suitable geometries. Commercially we have not been able to obtain GCA's with capillary radii smaller than  $0.5 \mu\text{m}$ . [12] However, even if one were to produce smaller capillaries, they would be only of limited use. The reason for this is that a comparison with theory will be easiest in the range of  $t$  where the bulk system shows a strong powerlaw divergence. This range often is referred to as the "critical region". It is known that the correlation-length amplitude  $\xi_0$  is only weakly dependent on pressure. [26] Thus one expects a given  $L$  to produce a finite-size-affected range of  $t$  which is nearly pressure independent. On the other hand, from Fig. 1 it is clear that the critical region for the *dynamics* is strongly pressure dependent. At high pressure it is restricted to  $t \lesssim 3 \times 10^{-4}$ , whereas at vapor pressure it covers the range  $t \lesssim 3 \times 10^{-3}$ . Thus it is desirable to use geometries with characteristic capillary radii which are large enough for the finite-size effects to occur for  $t \lesssim 3 \times 10^{-4}$ . Examination of the  $1 \mu\text{m}$  data (see below) shows that the finite-size region extends over the range  $t \lesssim 10^{-4}$ . Assuming the scaling of Eq. 6, we conclude that the finite-size region will be about as wide as the critical region at the higher pressures when  $L \simeq 0.5 \mu\text{m}$ , and that the amount of useful information obtainable diminishes as  $L$  decreases below half a  $\mu\text{m}$ . Thus our only real option for covering a wide range of  $L$  is to go to *large*  $L$ . However, for large  $L$  the finite-size effects of interest occur very close to  $T_\lambda$  where the sample inhomogeneity due to the Earth's gravitational acceleration has a significant influence.

The gravity effect is illustrated in Fig. 2 in terms of the phase diagram of  $^4\text{He}$ . The  $\lambda$  line, along which the liquid undergoes a transition from a superfluid (He-II) to a normal (Navier-Stokes) liquid (He-I), extends from 2.172 K at vapor pressure (0.05 bar) to 1.763 K at the melting pressure (30.13 bar) [27,28]. The inhomogeneity induced by gravity [13] is due to the hydrostatic pressure which varies with height in the liquid. This pressure variation has the effect of inducing a vertical spatial variation of the transition temperature. This is illustrated in more detail in the right portion of Fig. 2. If the sample top is at a pressure  $P = P_0$ , then the bottom will be at  $P = P_0 + \rho gh$  where  $\rho$  is the fluid density,  $g$  the gravitational acceleration, and  $h$  the sample height. Over

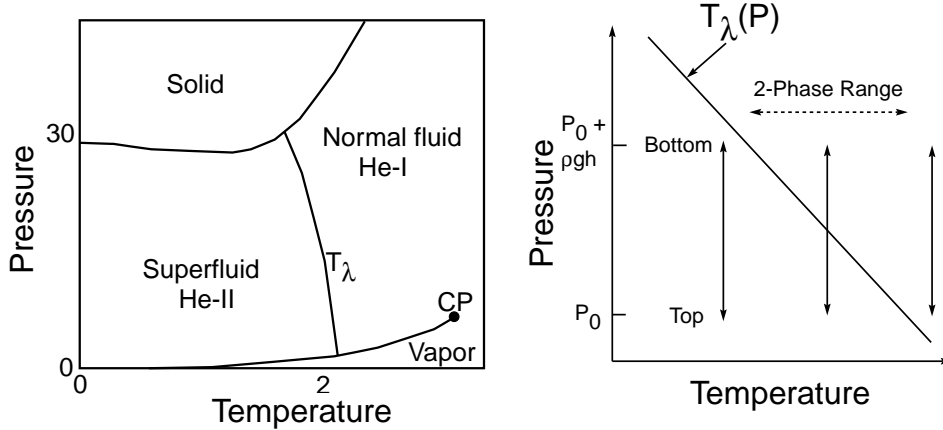


Fig. 2. Schematic phase diagram of  ${}^4\text{He}$ , and an illustration of the gravity effect. this pressure range the transition temperature  $T_\lambda(P)$  varies significantly. The parameter  $\beta \equiv -(\partial T/\partial z)_\lambda$  is given by

$$\beta = -\rho g(\partial T/\partial P)_\lambda \quad (9)$$

and provides a quantitative measure of the severity of the gravity effect. Values of  $\beta(P)$ , in  $\mu\text{K}/\text{cm}$ , are given in Fig. 3. One sees that, for a typical sample of size 1 cm at SVP, one has a two-phase region over a temperature interval of  $1.27 \mu\text{K}$ . Thus it is not possible to approach the transition more closely on average than within a  $\mu\text{K}$  or so. At higher pressures  $\beta(P)$  increases because the slope of the  $\lambda$ -line  $(\partial P/\partial T)_\lambda$  decreases and the density increases. At 30 bar the two-phase region for a sample of a given height would be wider by a factor of 2.5. Of course the effect of gravity on the average measured properties extends well beyond the two-phase region.

Associated with the distribution of transition temperatures is a more subtle “averaging” over a vertical range  $\xi_g$  of the properties due to the growth of the correlation length near the *local* transition. Thus the local properties are no longer those of the three-dimensional bulk transition. This effect is discussed in more detail in Sect. 6 below. For most experiments it is smaller than the effect due to the variation of  $T_\lambda(z)$  over the sample height  $h$ .

Returning to the finite-size samples, it turns out that helium at SVP and in cylinders with  $L \gtrsim 8 \mu\text{m}$  can not be studied effectively on Earth because the gravitational “rounding” of the resistivity will become significant compared to the expected finite-size rounding. At  $P = 30$  bar, gravitational rounding becomes a problem already for  $L \simeq 3.5 \mu\text{m}$ . This will be discussed more quantitatively below in Sect. 6. In microgravity the maximum useable size is limited only by the experimental temperature resolution, and is near  $50 \mu\text{m}$ . Thus the microgravity experiment can add a factor of 6 to 14 in  $L$  (depending on the pressure) to the size range accessible on Earth. We note that a factor of 6 (14)

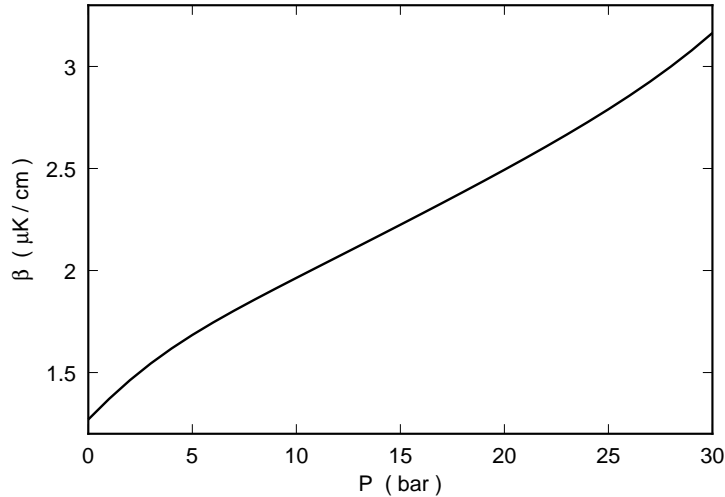


Fig. 3. The width per cm of sample height of the temperature range of isothermal coexistence of He-I and He-II (the two-phase region) as a function of the pressure. The values are for the gravitational acceleration on the Earth’s surface.

in  $L$  is a factor of 15 (50) for the scaling variable  $X$ .

## 4 Analysis of existing data

### 4.1 Conductivity of Bulk $^4\text{He}$

An effective evaluation of the finite-size thermal conductivity of  $^4\text{He}$  near  $T_\lambda$  requires an accurate knowledge of the bulk conductivity  $\lambda$ . The bulk conductivity was measured by several authors.[14–17] We will use the data by Tam and Ahlers[16] for their “Cell F” (TA) because they cover a very wide range of reduced temperatures, and because they are the only set we know of which covers several isobars in addition to saturated vapor pressure (SVP).

The SVP and 28 bar data for  $\lambda$  were shown already in Fig. 1 over a wide range of  $t$ . They extend from  $t \simeq 3 \times 10^{-6}$  to  $t \simeq 1.0$ . The large- $t$  data are necessary for the evaluation of the finite-size data because the bulk and finite-size measurements must be normalized to each other in a region where finite-size effects are negligible, as will be described in Sect. 4.2. For small  $t$  the bulk data are shown in the form of the resistivity on logarithmic scales in Fig. 4. Deviations from fits of the powerlaw

$$R = R_0 t^x \tag{10}$$

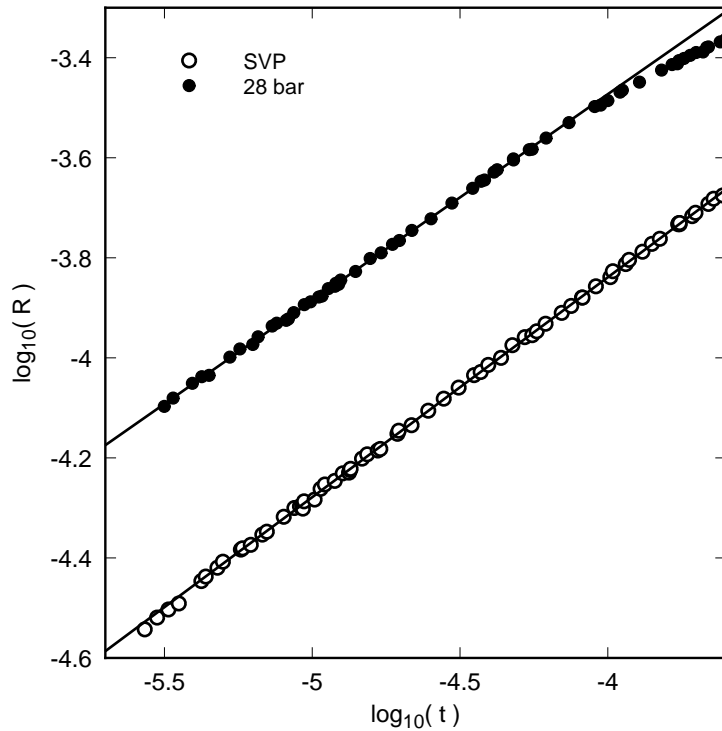


Fig. 4. The resistivity  $R = 1/\lambda$  in the critical region for bulk helium at SVP (open circles) and at 28 bar (solid circles) on logarithmic scales. The solid lines are power-law fits to the data for  $t < 2 \times 10^{-4}$  at SVP and  $t < 8 \times 10^{-5}$  at 28 bar.

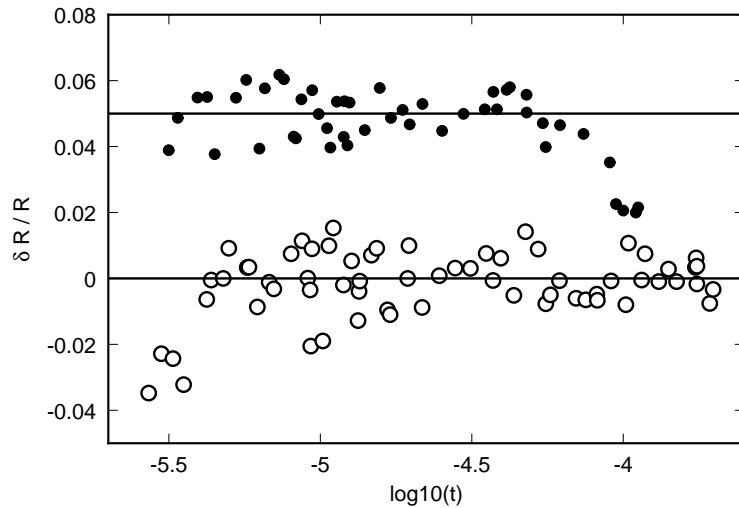


Fig. 5. Relative deviations  $\delta R/R$  from the fits shown in Fig 4 and given by Eqs. 10 to 12. The upper set of data (solid circles) is for  $P = 28$  bar and has been shifted up by 0.05. The lower set (open circles) is for SVP.

to these data are shown in Fig. 5. The fits yielded the parameters

$$R_0 = 8.312 \times 10^{-3} \text{ cmKs/erg}, \quad x = 0.4397 \quad (11)$$

at saturated vapor pressure and

$$R_0 = 1.507 \times 10^{-2} \text{ cmKs/erg}, \quad x = 0.4127 \quad (12)$$

at  $P = 28$  bar. An analysis at all pressures where measurements exist [18] (0.05, 6.85, 14.73, 22.30, and 28.00 bar) yielded exponents which could, within their uncertainty, be represented by

$$x = 0.4395 - 0.000994P \quad (13)$$

where  $P$  has the units bar. Fits of the data with the exponent fixed at that given by Eq. 13 gave  $R_0 = 0.00831, 0.00974, 0.01107, 0.01302,$  and  $0.01498$  cm K s / erg for the five isobars. In the calculations of finite-size and gravity effects given below we will use  $x$  as given by Eq. 13 and  $R_0$  given by linear interpolation between the values given here.

#### 4.2 Conductivity of $^4\text{He}$ in $1\text{-}\mu\text{m}$ radius GCAs

Here we examine in some detail the KA results [11] for the conductivity of  $^4\text{He}$  at SVP in GCAs with capillary radii of  $1 \mu\text{m}$ . It was not possible to determine the effective area of the helium with sufficient accuracy. In addition, the parallel conduction through the cell wall, the glass, and the epoxy used to seal the GCA to the wall was not measured independently. Therefore the parallel conduction and the length-to-area ratio  $h/A = 0.39 \text{ cm}^{-1}$  were obtained by adjusting them so as to cause the helium conductivity to agree with the TA data in the temperature range  $7 \times 10^{-4} \lesssim t \lesssim 6 \times 10^{-3}$ . In this range, which is shown in Fig. 6 by the solid horizontal bar, the finite-size effect on  $\lambda$  is expected to be negligibly small. The results are shown over a wide range of  $t$  in Fig. 6. The solid circles are the TA bulk data, and the open ones are the results for the finite geometry. As  $T_\lambda$  is approached, the finite-size effect becomes apparent. The data for the restricted geometry do not diverge like the bulk data, and instead approach a finite value as  $t$  vanishes.

Data for  $R$  in the finite-size-affected region of  $t$  are shown on linear scales in Fig. 7. They reveal a rounded transition, with no evidence of a singularity, as would be expected for a one-dimensional system. Above  $T_\lambda$  the finite-size effect on  $R$  extends to quite large values of  $t$ . This is characteristic of the

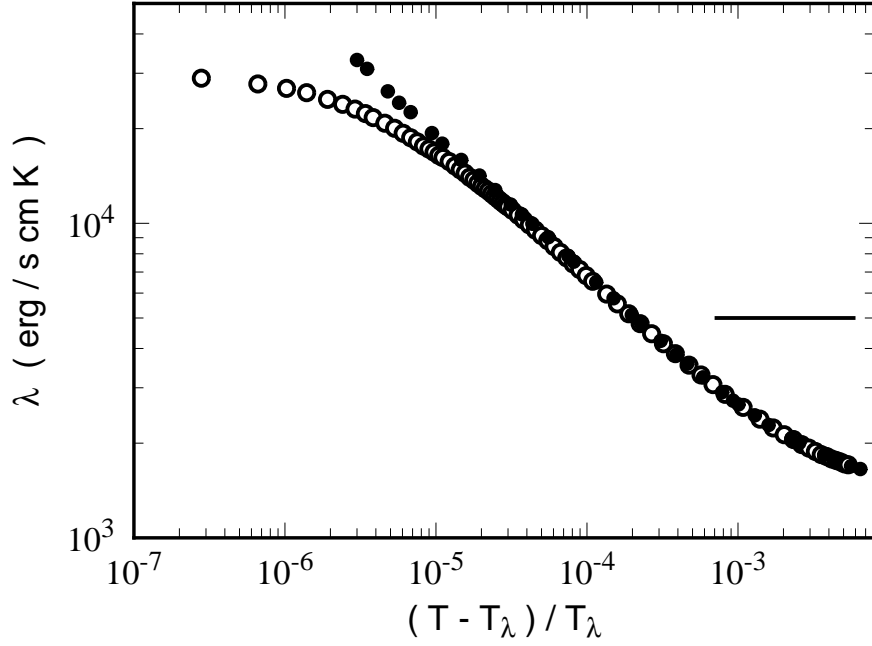


Fig. 6. The thermal conductivity at SVP for bulk helium (solid circles) and for helium in a GCA with pore radii of  $1 \mu\text{m}$  (open circles). The horizontal bar shows the range of  $t$  over which the finite-size data were fit to the bulk data by adjusting the parallel (“wall”) conduction and the area-to-length ratio.

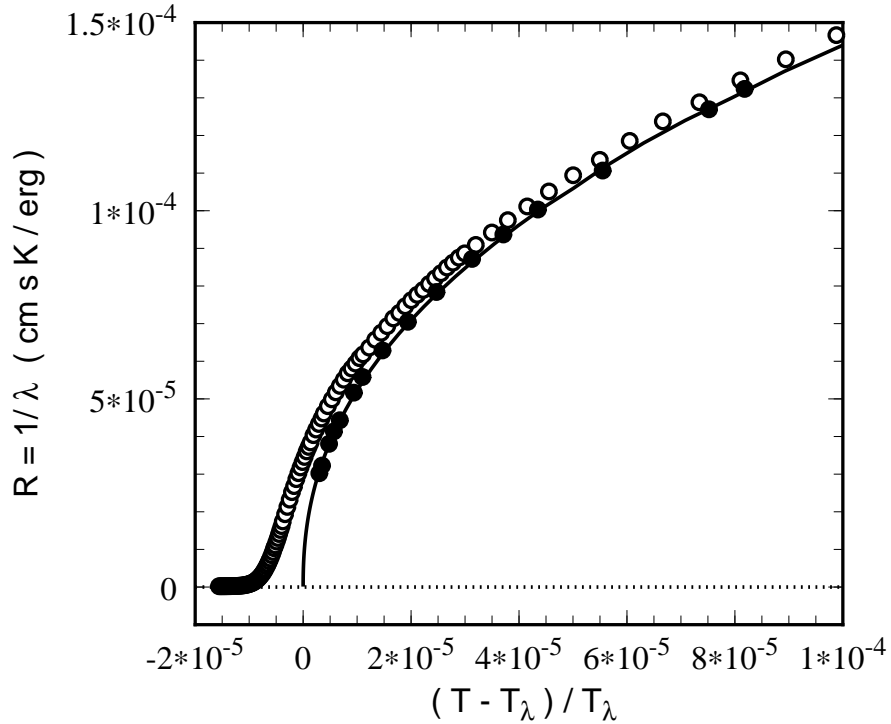


Fig. 7. The thermal conductivity at SVP for bulk helium (solid circles) and for helium in a GCA with pore radii of  $1 \mu\text{m}$  (open circles) in the finite-size region on linear scales. The solid line is the fit Eqs. 10 and 11 to the bulk data.

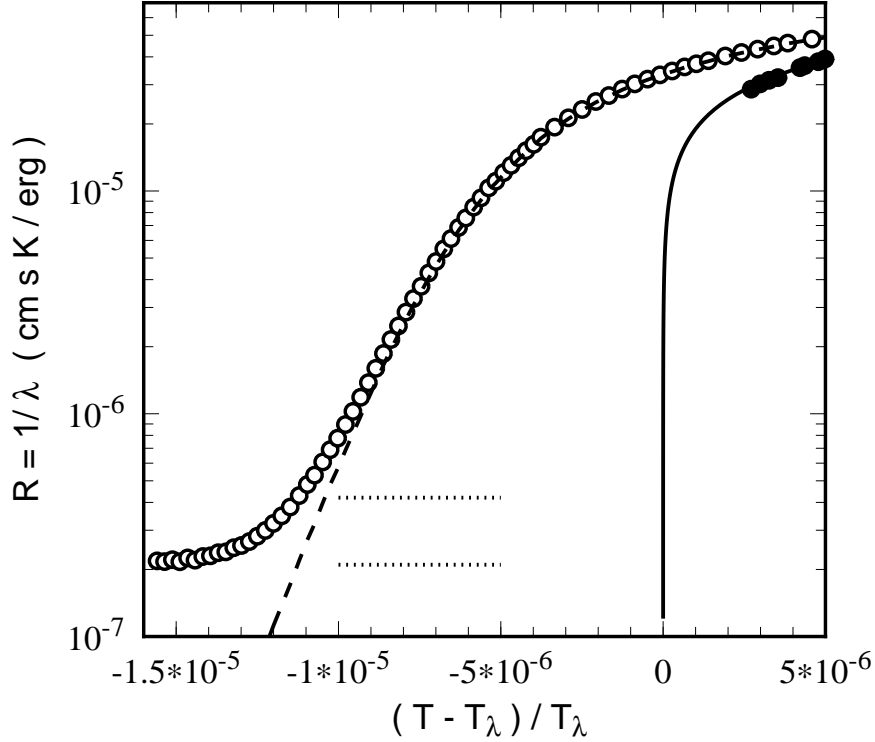


Fig. 8. The thermal resistivity  $R$  close to  $T_\lambda$  at SVP for bulk helium (solid circles) and for helium in a GCA with pore radii of  $1 \mu\text{m}$  (open circles). The vertical scale is logarithmic and the horizontal one is linear. The solid line is the fit Eq. 10 to the bulk resistivity. The dashed line is  $R(t, L)$  after subtraction of the boundary contribution.

surface contribution to finite-size effects, as seen in static properties. Below  $T_\lambda$  ( $t < 0$ ),  $R(t, L)$  approaches zero rather more rapidly.

The behavior below  $T_\lambda$  is shown in more detail in Fig. 8. One sees that  $R$  reaches a finite value as  $t$  decreases. This saturation is due to the series resistance of the copper end plates of the conductivity cell and to the series boundary resistance which had not been subtracted. It corresponds to an effective boundary resistivity  $R_b = 2.1 \times 10^{-7} \text{ cm s K / erg}$ . When  $R_b$  is subtracted, the data yield the dashed line in the figure. One sees that the dependence of  $R$  on  $t$  at low temperatures is consistent with an exponential decay of  $R$  as  $t$  decreases. The very rapid decrease of  $R$  with decreasing  $t$  permits its measurement only over a relatively narrow range of  $t$ . As a guide, the two horizontal dotted lines correspond to  $R_b$  and  $2R_b$ . At a reduced temperature of  $-1.1 \times 10^{-5}$ ,  $R(t, L)$  is about equal to  $R_b$  and for smaller  $t$   $R(t, L)$  soon ceases to be measurable. A fit of  $R(t, L)$  (after the subtraction of  $R_b$ ) to an exponential function gave

$$R/R_d = \exp(t/t_0) \quad (14)$$

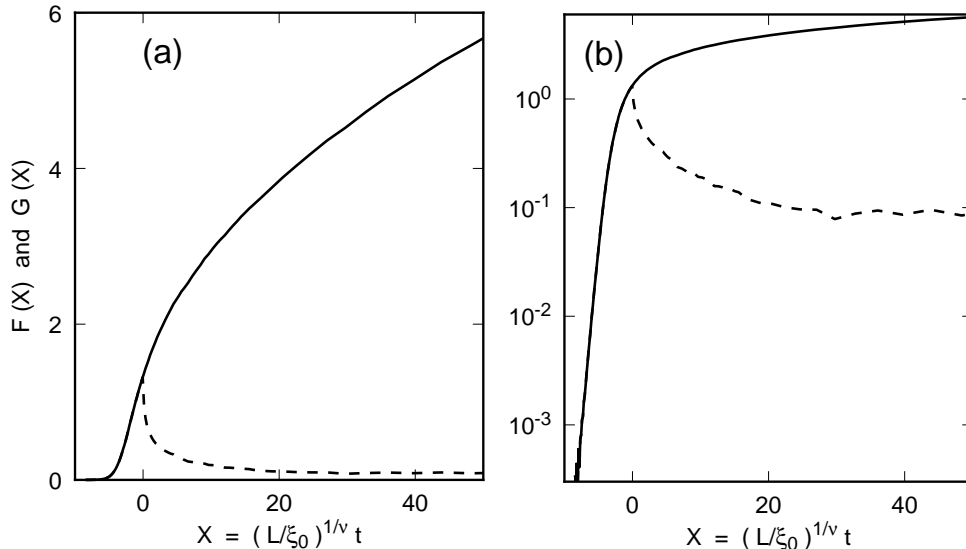


Fig. 9. The scaling functions  $F(X)$  and  $G(X)$  as a function of the scaling variable  $X = (L/\xi_0)^{1/\nu} t$ . (a) gives the scaling functions on a linear scale, and (b) gives them on a logarithmic vertical scale.

with  $R_d = 0.0052 \text{ s cm K / erg}$  and  $t_0 = 1.11 \times 10^{-6}$ . We note that in the assumed functional form Eq. 14 the argument of the exponential is linear in the absolute temperature  $T$ . Because of the narrow range of  $t$  over which the exponential decay of  $R$  can be measured, the data are not sufficient to rule out a somewhat different dependence upon  $T$ . Clearly it would be interesting to examine the behavior of  $R$  below  $T_\lambda$  theoretically, initially perhaps in the mean-field limit and in analogy to the known behavior of one-dimensional superconductors. A specific prediction could then be tested for consistency with the data. Of course it would be particularly interesting to see whether the scaling with  $\xi/L$  implied by Eq. 6 is consistent with the expected behavior.

#### 4.3 The Scaling Functions $F(X)$ and $G(X)$

In order to compute the scaling functions from the experimental data and Eqs. 6 and 8, we would like the amplitudes  $\xi_0$  of the correlation length above  $T_\lambda$ . The only direct experimental information about correlation-length amplitudes comes from measurements of the superfluid density below  $T_\lambda$  which give the transverse correlation-length amplitudes  $\xi_0^T$ . [26,29] With the theoretical value of the universal ratio[30]  $\xi_0/\xi_0^T$  they yield the amplitudes[32]

$$\xi_0 = 1.432 \times 10^{-10} \text{ m at SVP} \quad (15)$$

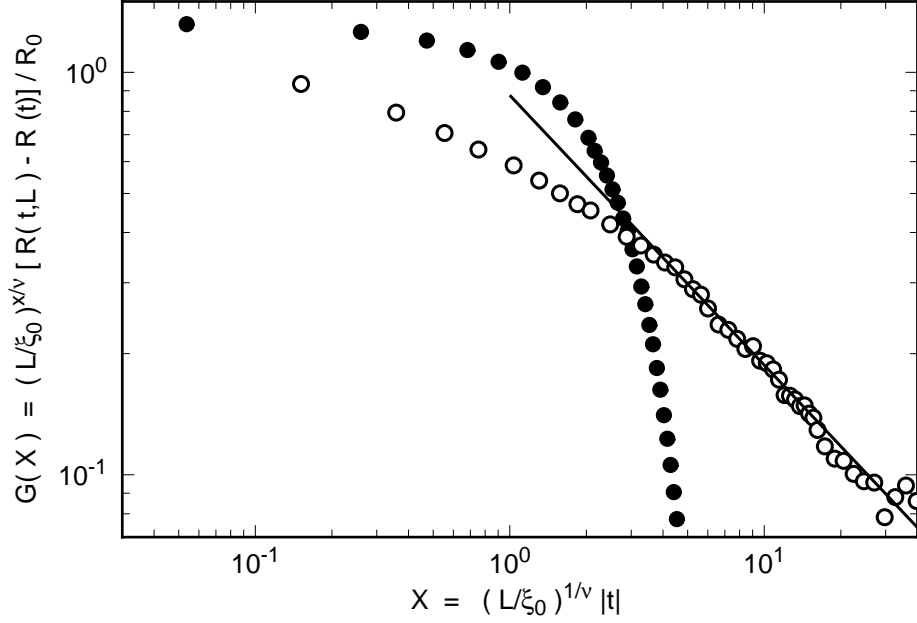


Fig. 10. The scaled excess resistivity  $G(X) = (L/\xi_0)^{x/\nu} [R(t,L) - R(t)]/R_0$  as a function of  $X = (L/\xi_0)^{1/\nu} |t|$  on logarithmic scales. Open circles:  $T > T_\lambda$ . Solid circles:  $T < T_\lambda$ . The solid line has a slope of  $-\nu$ .

and

$$\xi_0 = 1.314 \times 10^{-10} \text{ m at } P = 28 \text{ bar} \quad (16)$$

above  $T_\lambda$ . Thus for the  $1 \mu\text{m}$  capillaries of the KA experiment at SVP we have  $L/\xi_0 = 7 \times 10^3$ . Figure 9 shows  $F(X)$  and  $G(X)$  computed from the KA data, using Eqs. 10 and 11 for the infinite-system resistivity  $R(t)$ . In Fig. 9a  $F$  and  $G$  are given on linear scales as a function of  $X$ . Figure 9b gives the same information, but the logarithmic vertical scale reveals the behavior more clearly when the functions become small.

In Fig. 10 we show the scaling variable  $G(X)$  (Eq. 8) as a function of  $X$  for both sides of the bulk transition as a function of  $|t|$  on logarithmic scales. Above  $T_\lambda$  (open circles) and for  $X \gtrsim 3$ , the excess resistivity is consistent with a surface contribution given by a powerlaw with an exponent equal to that of the correlation length  $\xi$  (Eq. 3). The solid line in the figure corresponds to

$$G(X) = G_0 X^{-\nu} \quad (17)$$

with  $G_0 = 0.88$ . A powerlaw clearly is not the right description of the excess resistivity below  $T_\lambda$  (solid circles) where, as we saw, an exponential decay gives a better fit.

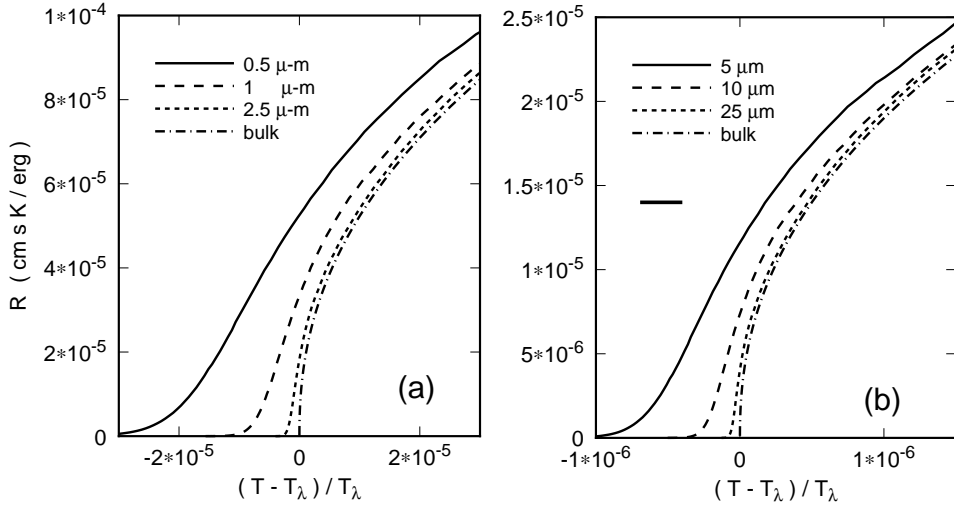


Fig. 11. Estimates based on the scaling function  $F(X)$  of the thermal resistivity  $R(t, L)$  of  $^4\text{He}$  at SVP in cylindrical tubes of the various radii  $L$  given in the figure. The horizontal bar in (b) shows the width of the two-phase region for a sample height  $h = 5$  mm.

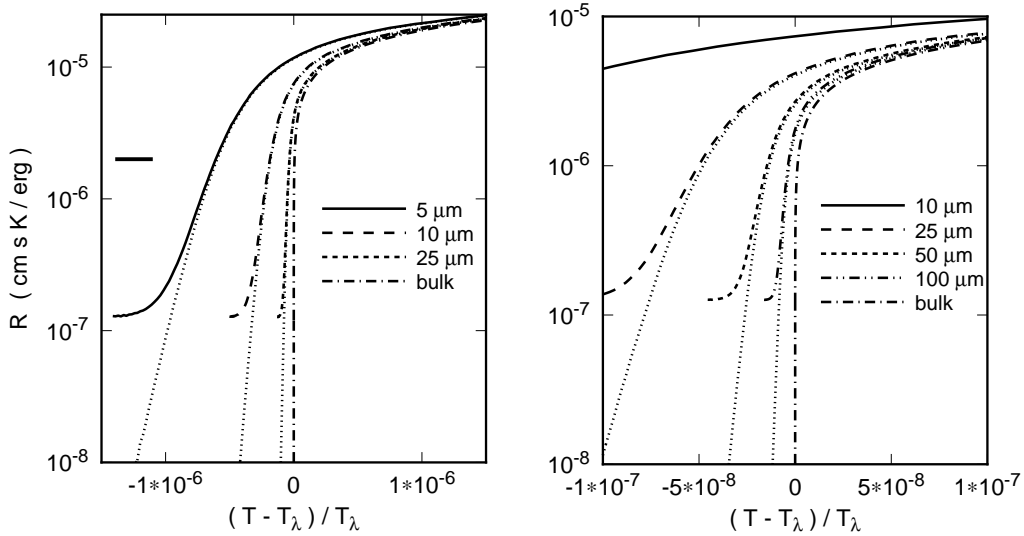


Fig. 12. Estimates based on the scaling function  $F(X)$  of the thermal resistivity  $R(t, L)$  of  $^4\text{He}$  at SVP in cylindrical tubes of the various radii  $L$  given in the figure. Here the vertical scale is logarithmic. The saturation at small  $t$  is due to the boundary resistance. The dotted lines show the corresponding predictions without the boundary contribution. The horizontal bar in (a) shows the width of the two-phase region for a sample height  $h = 5$  mm. On the scale of (b) this two-phase region would be wider than the figure.

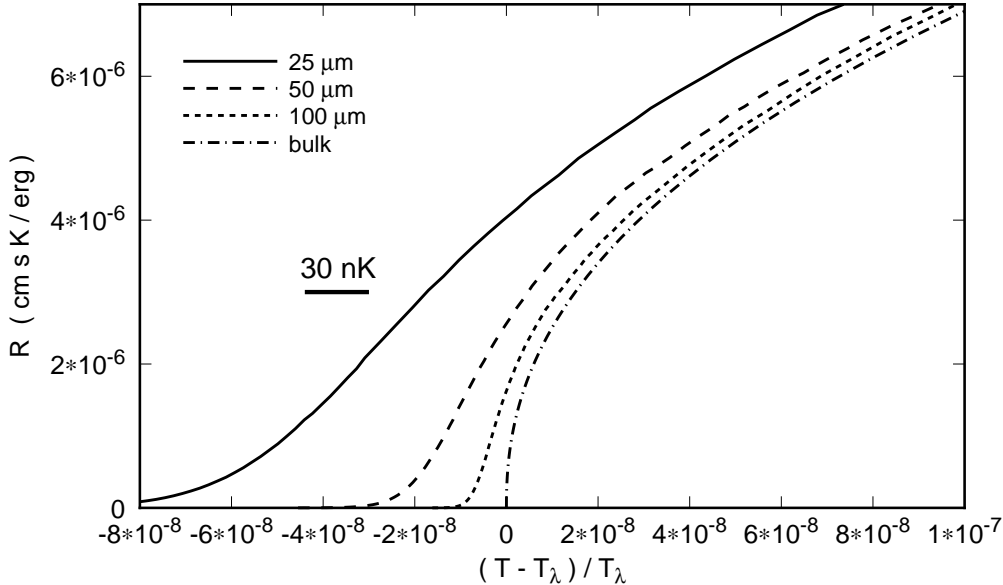


Fig. 13. Estimates based on the scaling function  $F(X)$  of the thermal resistivity  $R(t, L)$  of  $^4\text{He}$  at SVP in cylindrical tubes of the various radii  $L$  given in the figure. The horizontal bar shows a temperature increment of 30 nK.

## 5 Predictions, and parameter choices for new experiments

### 5.1 Saturated Vapor Pressure

For a given  $L$ ,  $\xi_0$ , and  $R(t)$  Eqs. 6 to 8 are easily solved for  $R(t, L)$  and thus yield a prediction of the finite-size effect on  $R$  at any size  $L$ . Some examples for SVP are given in Figs. 11 to 13. These estimates are helpful in making optimal choices of experimental parameters. We must emphasize, however, that the predictions are based on the assumption of the validity of finite-size scaling for transport properties. Thus the possibility that the experimental results will turn out to be inconsistent with Figs. 11 to 13 can not be ruled out at this time.

One issue is the sample thickness  $h$ . In order to minimize the effect of the boundary resistance  $R_b$  in series with the sample, a relatively large value of  $h$  is desirable. On the other hand, thermal relaxation times become excessively long when  $h$  is too large. An optimal choice is in the range from 3 to 5 mm. In Fig. 12 we show on a vertical logarithmic scale the expected effect of  $R_b$  on measurements in a  $h = 5$  mm sample (on the linear scale of Figs. 11 and 13 the effect of  $R_b$  is not noticeable). Regardless of  $L$ , the boundary resistance imposes about the same limitation on the measurement of the exponential decay of  $R$  at small  $t$ . However, for the smaller values of  $L$  the largest thickness available commercially is one mm. For this reason the behavior of  $R$  at small  $t$  will be

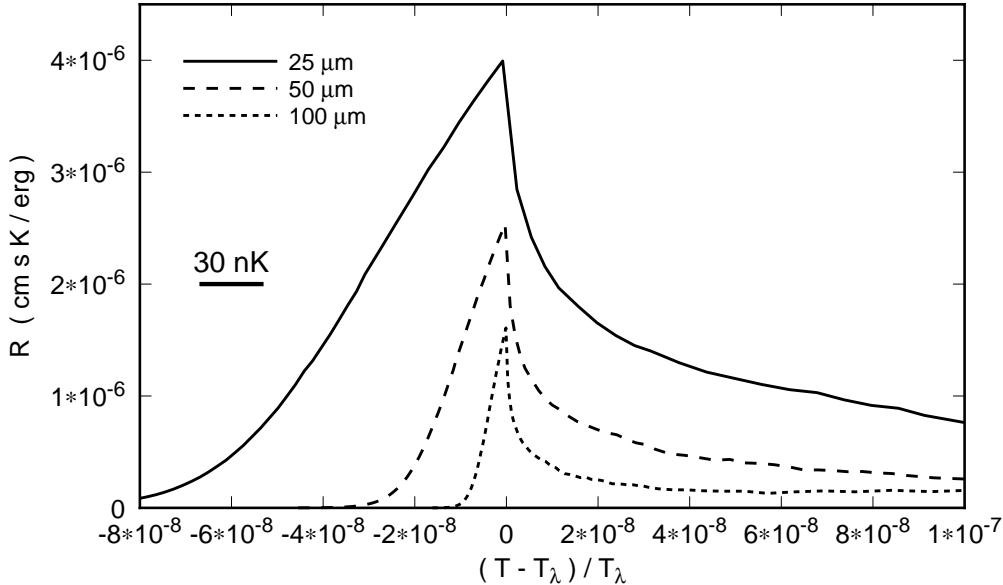


Fig. 14. Estimates based on the scaling function  $G(X)$  of the excess thermal conductivity  $R(t, L) - R(t)$  of  ${}^4\text{He}$  in cylindrical tubes of the various radii  $L$  given in the figure. The horizontal bar shows a temperature increment of 30 nK.

somewhat less accessible to measurement for the smallest values of  $L$ .

In Figs. 11b and 12a we show as a small horizontal bar the width of the two-phase region for a sample of height 5 mm and at SVP. The figures suggests that the finite-size effect for  $L \lesssim 5\mu\text{m}$  is spread over a range of  $t$  which is much wider than the width of the two-phase region, and that the effect of gravity should thus be relatively unimportant. In the range  $5 < L < 10\mu\text{m}$  a detailed calculation is necessary to assess the importance of gravity, and this will be provided below in Sect. 6. For significantly larger samples microgravity experiments will clearly be necessary. Assuming that there will be only one such experiment, it remains to choose the optimal size for this purpose. On the one hand,  $L$  should be as large as possible so as to yield the largest possible total range of  $L$  over which information will become available. On the other hand, if  $L$  is too large, then the finite-size effects will occur so close to  $T_\lambda$  that they can no longer be resolved quantitatively even with modern ultra-high resolution thermometry. We show the three examples  $L = 25, 50,$  and  $100\mu\text{m}$  in Fig. 13. To provide additional detail, we show  $R(t, L) - R(t)$  in Fig. 14. On the basis of the experience with CHeX, [9] it seems reasonable to expect that temperature differences  $\Delta T$  across our cell can be measured with a resolution of perhaps  $3 \times 10^{-10}$  K even when a relatively large bandwidth is employed to permit discrimination against particle heating. Thus a measurement with a resolution of one % would require  $\Delta T \simeq 30$  nK if only the raw data are used. A temperature increment of this size is shown in Figs. 13 and 14 as small horizontal bars. It is clearly adequate to resolve the predicted finite-size effect for  $L = 25\mu\text{m}$ . Signal averaging should improve the resolution by a significant

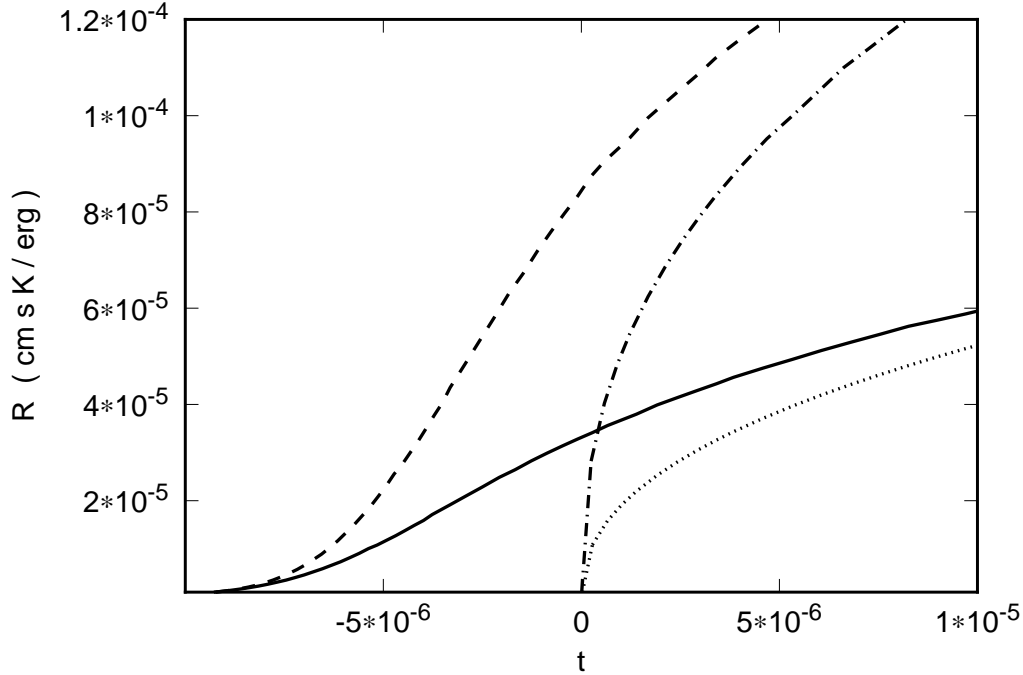


Fig. 15. Estimates based on the scaling function  $G(X)$  of the thermal conductivity  $R(t, L)$  of  ${}^4\text{He}$  in cylindrical tubes with  $L = 1\mu\text{m}$ . The dotted and solid lines are for SVP, and the dash-dotted and dashed curves are for  $P = 28$  bar.

factor. Thus we feel that the  $L = 50\mu\text{m}$  geometry can still yield quantitative data. However, based on Figs. 13 and 14 we believe that  $L = 100\mu\text{m}$  is too large.

## 5.2 Pressure Dependence

As was discussed near the end of Sect. 2, we do not expect strict universality along the  $\lambda$ -line of the functions  $F(X)$  and  $G(X)$  as defined by Eqs. 6 and 8 because the powerlaw Eq. 10 used for the bulk system is only an effective powerlaw which does not conform to universality. Nonetheless, the difference function  $G(X)$ , together with  $R(t)$  for the bulk system at the elevated pressure, should provide a good indication of the magnitude of the finite-size effect. We have used it to compute the results shown in Fig. 15. The dash-dotted and dotted lines are for bulk helium for  $P = 28$  bar and SVP respectively. The dashed and solid lines are the corresponding results for  $L = 1\mu\text{m}$ . At the higher pressure the finite-size effect appears larger; but actually it is larger only in proportion to the size of  $R(t)$ . The width along the temperature axis over which the finite-size effect is significant is nearly pressure independent, as was expected because  $\xi_0$  does not change much with  $P$ .

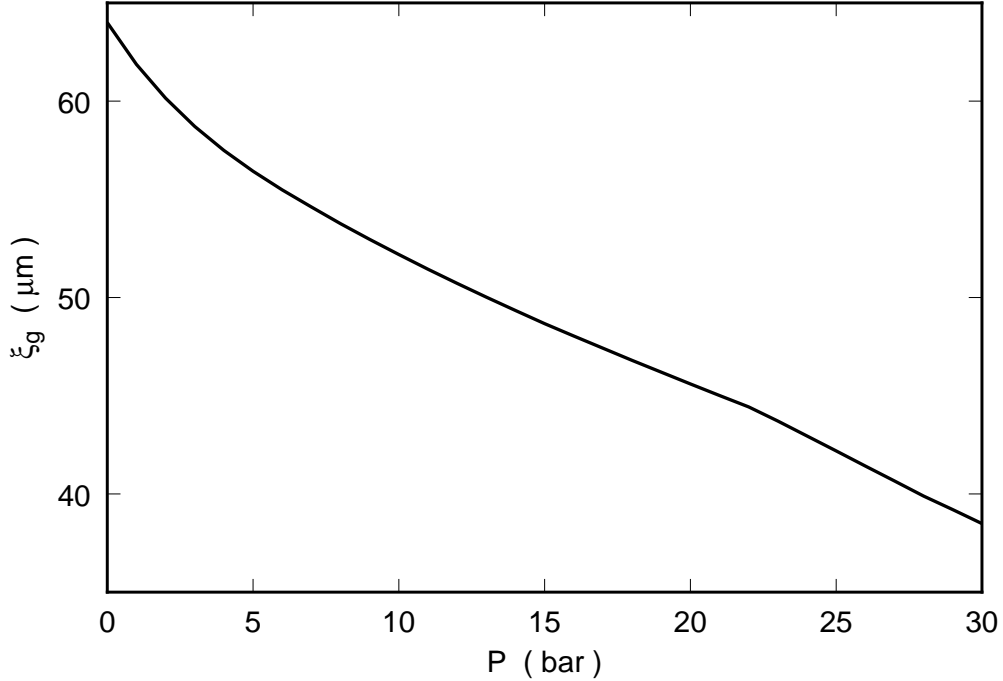


Fig. 16. The saturation length  $\xi_g$  as a function of the pressure  $P$ .

## 6 Quantitative Evaluation of the Gravity Effect

Here we present a quantitative estimate of the effect of gravity for various cylinder radii and pressures. We can roughly divide the gravity effect into two components. Approximately, one can assume that the sample locally has bulk properties which are determined by a height dependent transition temperature  $T_\lambda(z)$  and the local temperature  $T(z)$ . In this local approximation the average resistivity  $\bar{R}(L, \bar{t})$  for instance can be obtained by numerical integration over the sample height. This approximation neglects the fact that the neighboring layers of the fluid influence each other's properties because of a proximity (vertical averaging) effect associated with the dramatic growth of the correlation length as  $T_\lambda(z)$  is approached. An estimate of this proximity effect suggests that the local correlation length, instead of diverging, will in the presence of gravity saturate at a value determined by the relationship[33]

$$\xi_g = \xi_0 [(1/T_\lambda)(\partial T/\partial z)_\lambda \xi_g]^{-\nu} \quad (18)$$

which yields

$$\xi_g = \xi_0^{1/(1+\nu)} [(1/T_\lambda)(dT_\lambda/dz)]^{-\nu/(1+\nu)}. \quad (19)$$

At SVP one finds  $\xi_g \simeq 64\mu\text{m}$ , which is equivalent to the length  $\xi$  for the homogeneous system near  $t_g \simeq 4 \times 10^{-9}$ . Although  $\xi_0$  varies only slightly with

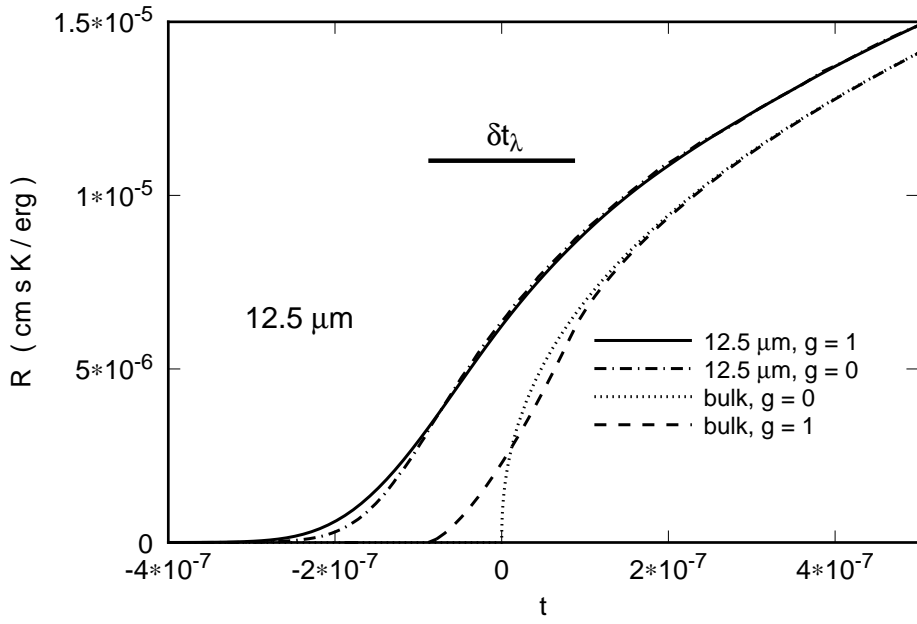


Fig. 17. Estimates of the resistivity for a sample at SVP, of height  $h = 3$  mm, and with  $L = 12.5\mu\text{m}$ , in the presence of gravity ( $g = 1$ ) and for  $g = 0$ . The case of bulk helium is shown for comparison. The horizontal bar shows the width  $\delta t_\lambda$  and location of the two-phase region for bulk helium.

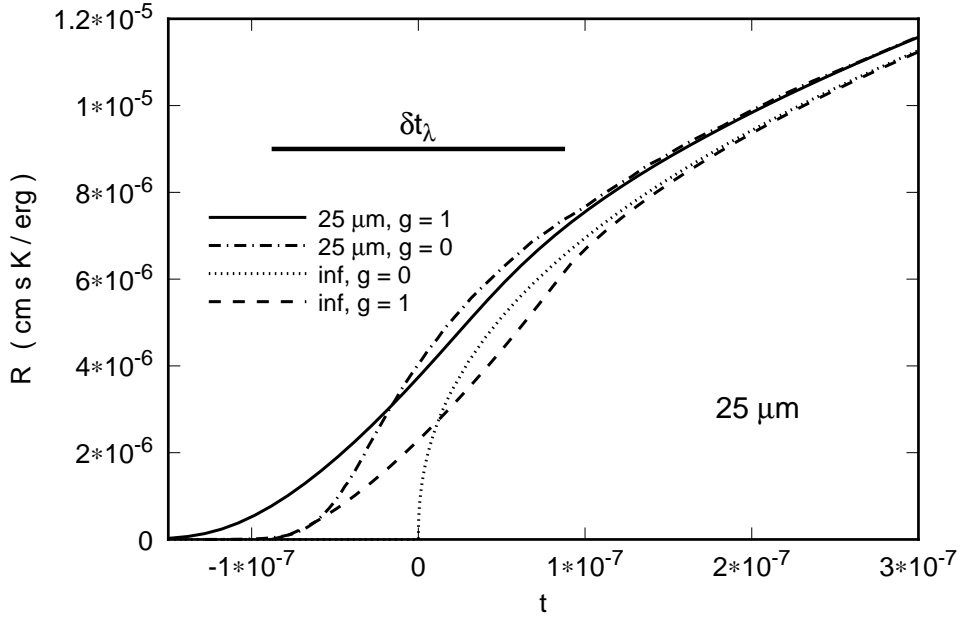


Fig. 18. Estimates of the resistivity for a sample at SVP, of height  $h = 3$  mm, and with  $L = 25\mu\text{m}$ , in the presence of gravity ( $g = 1$ ) and for  $g = 0$ . The case of bulk helium is shown for comparison. The horizontal bar shows the width  $\delta t_\lambda$  and location of the two-phase region for bulk helium.

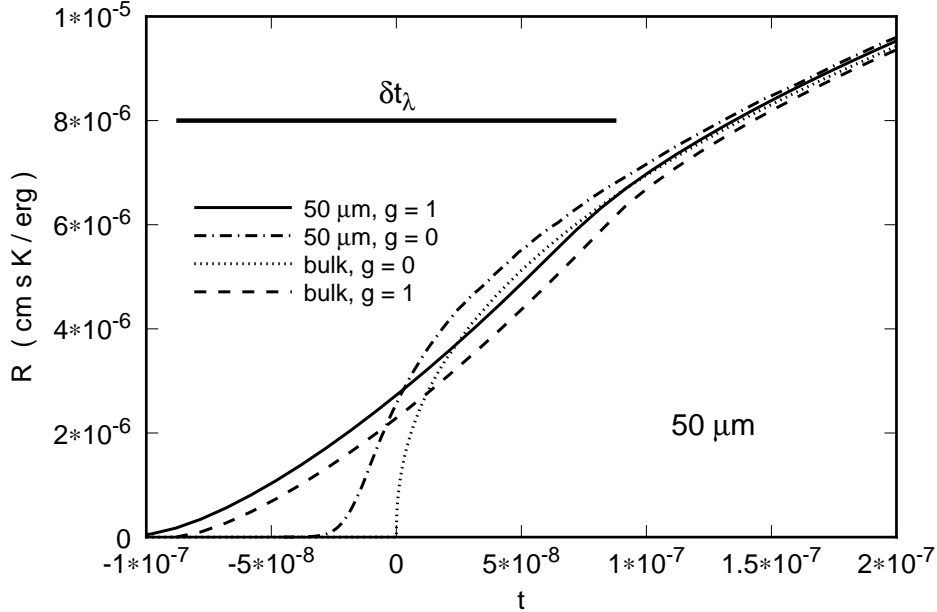


Fig. 19. Estimates of the resistivity for a sample at SVP, of height  $h = 3$  mm, and with  $L = 50\mu\text{m}$ , in the presence of gravity ( $g = 1$ ) and for  $g = 0$ . The case of bulk helium is shown for comparison. The horizontal bar shows the width  $\delta t_\lambda$  and location of the two-phase region for bulk helium.

$P$ ,  $\xi_g$  decreases to about  $38\mu\text{m}$  as  $P$  increases to 30 bar, as is shown in Fig. 16. This yields  $t_g \simeq 7 \times 10^{-9}$  at 30 bar, showing that the proximity effect becomes more severe as  $P$  increases. Roughly, one would expect the resistivity, as well as other singular properties, to also saturate at their value for the homogeneous system near  $t_g$ , and in principle this averaged local property value should be used in the integration over the sample height. It turns out that the error made by approximating the local properties by those of the homogeneous system is much smaller than the effect of integrating over the height of typically a few mm. Qualitatively this is clear from the fact that the width

$$\delta t_\lambda(P) = \beta h \quad (20)$$

of the two-phase region for bulk helium is typically one to two orders of magnitude larger than  $t_g$ . Thus for the present purpose we neglected the proximity effect, and used the properties of the homogeneous system in the averaging over the sample height.

We consider the case where a constant heat current per unit area  $Q$  passes through the sample from the bottom. For illustrative purposes we used a sample height  $h = 3$  mm, which is a convenient size[11] for ground-based measurements. We chose  $z = 0$  at the top and  $z = h$  at the bottom of the sample. For a fixed temperature  $T_0$  at the top, the temperature  $T(z)$  was computed by numerical integration of  $dT = -QRdz$  using  $R = R(t(z), L)$

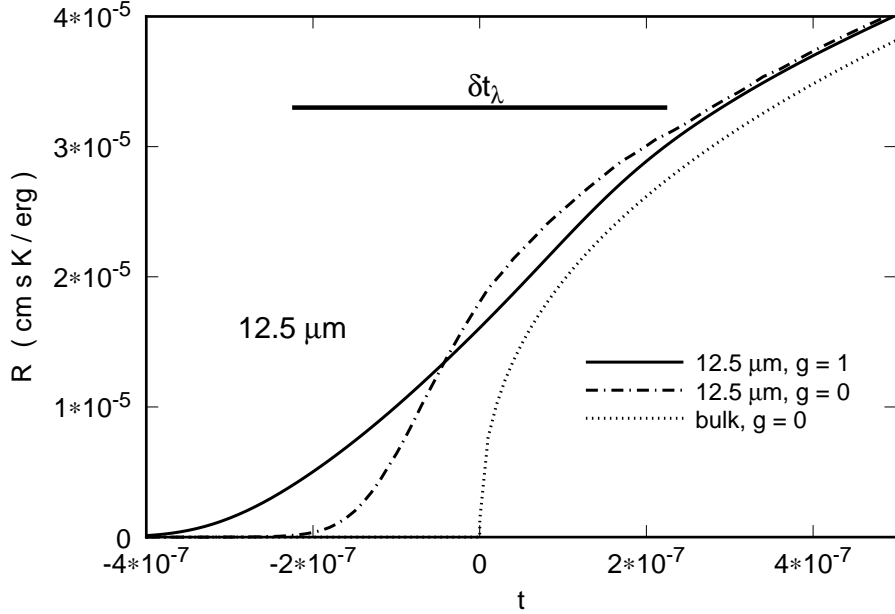


Fig. 20. Estimates of the resistivity in the presence of gravity ( $g = 1$ ) and for  $g = 0$  for a sample with  $P = 28$  bar and of height  $h = 3$  mm, with  $L = 12.5\mu\text{m}$ . The case of bulk helium is shown for comparison. The horizontal bar shows the width  $\delta t_\lambda$  and location of the two-phase region for bulk helium. Except for the pressure, this case is the same as the one shown in Fig 17. Note that the horizontal axis has the same scale as Fig 17, but that the scale of the vertical axis differs by a factor of about 2.7.

where  $t(z) = (T(z) - T_\lambda(z))/T_\lambda$ . The final temperature difference  $\Delta T$  across the sample was used to compute  $\bar{R} = \Delta T/(-Qh)$ . The result was assigned to a reduced temperature  $\bar{t} = (T_0 + \Delta T/2 - T_\lambda(h/2))/T_\lambda$ . With these choices, we have  $\bar{t} = 0$  when, for bulk helium and  $Q = 0$ , the interface between He-I and He-II is located at  $z = h/2$ . The calculation includes both the gravity effect and “curvature effects” [34] due to using a finite current. For the present calculations  $Q = 10^{-10}$  W/cm<sup>2</sup> was used and curvature effects were negligible. In an actual experiment  $Q$  is likely to be larger, and curvature corrections may be required.

In Figs. 17 to 19 the results at SVP are shown for  $L = 12.5, 25,$  and  $50 \mu\text{m}$  in the presence of gravity and for  $g = 0$ . As a reference, the results for bulk helium are repeated in each figure. The  $g = 0$  case for bulk is always shown as a dotted line. The bulk case in the presence of gravity is given by the simple dashed lines. The width  $\delta t_\lambda$  of its two-phase region is readily discerned and is given explicitly by the horizontal bar in each figure. The results for the finite geometry in the presence of gravity are shown as solid lines. For  $g = 0$  they are given as dash-dotted lines. Figure 17 suggests that gravity is surprisingly unimportant even for  $L$  as large as  $12.5 \mu\text{m}$ . To some extent this is illusory, as we shall see below. Nonetheless, the effect on the bulk system appears to be

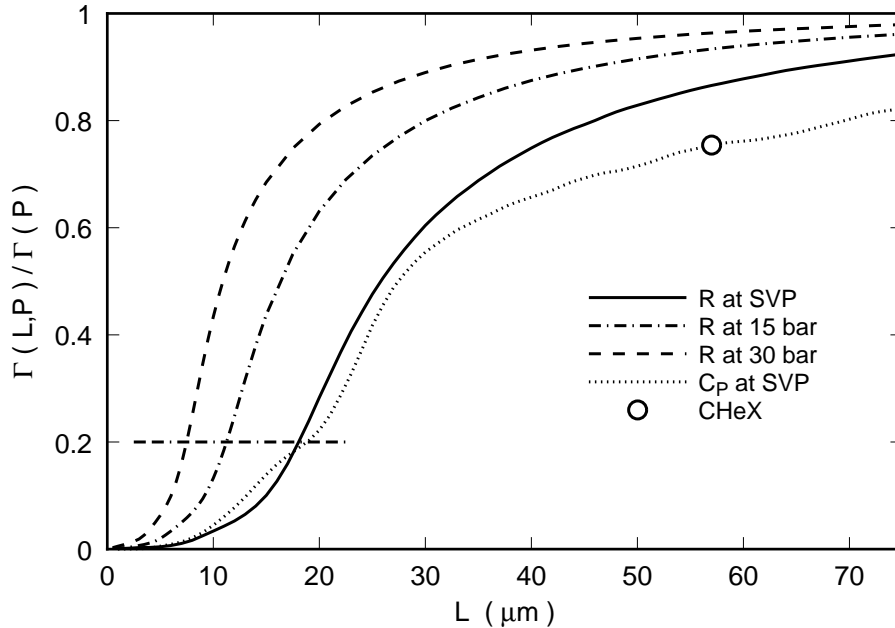


Fig. 21. The parameter  $\Gamma(L, P)/\Gamma(P)$  defined by Eq. 21 as a function of  $L$  for three different pressures. Also shown is the equivalent result for  $C_P$  at SVP, based on the CHeX results for the parallel-plate geometry.

much larger. The reason is of course that the bulk  $R$  has a singularity and thus varies rapidly as a function of  $h$ , whereas  $R(t, L)$  is smooth and varies relatively slowly near  $T_\lambda$ . Nonetheless, when  $L$  is increased to  $25 \mu\text{m}$ , the gravity effect on  $R(t, L)$  becomes quite obvious and ground-based measurements could not be accurately corrected to the gravity-free case. For  $L = 50 \mu\text{m}$  (Fig. 19) gravity is the major "rounding" effect and the finite-size effect is much smaller.

As the pressure is increased, the gravity effect becomes significantly larger because the slope of  $T_\lambda(P)$  decreases and the density increases (see Eq. 9). In Fig. 20 we show results for  $L = 12.5 \mu\text{m}$  equivalent to those shown in Fig. 17, but for  $P = 28$  bar. Whereas at SVP the gravity effect for  $L = 12.5 \mu\text{m}$  was modest, at  $P = 28$  bar it is overwhelming.

In order to quantify the extent of the gravity effect, we define the parameter

$$\Gamma^2(L, P) = \frac{\int_{-t_\lambda/2}^{t_\lambda/2} [R_g(t, L) - R_0(t, L)]^2 dt}{\int_{-t_\lambda/2}^{t_\lambda/2} R_0^2(t, L) dt} \quad (21)$$

where  $R_g$  and  $R_0$  are the resistivity in the presence of gravity and for  $g = 0$  respectively. We find that  $\Gamma(P) \equiv \Gamma(\infty, P) \simeq 0.278$  regardless of  $P$ . In Fig. 21 we show  $\Gamma(L, P)/\Gamma(P)$  as a function of  $L$  for three different pressures. We would like to divide the  $P - L$  plane into two regions, one in which gravity is relatively unimportant and another in which gravity has a dominating

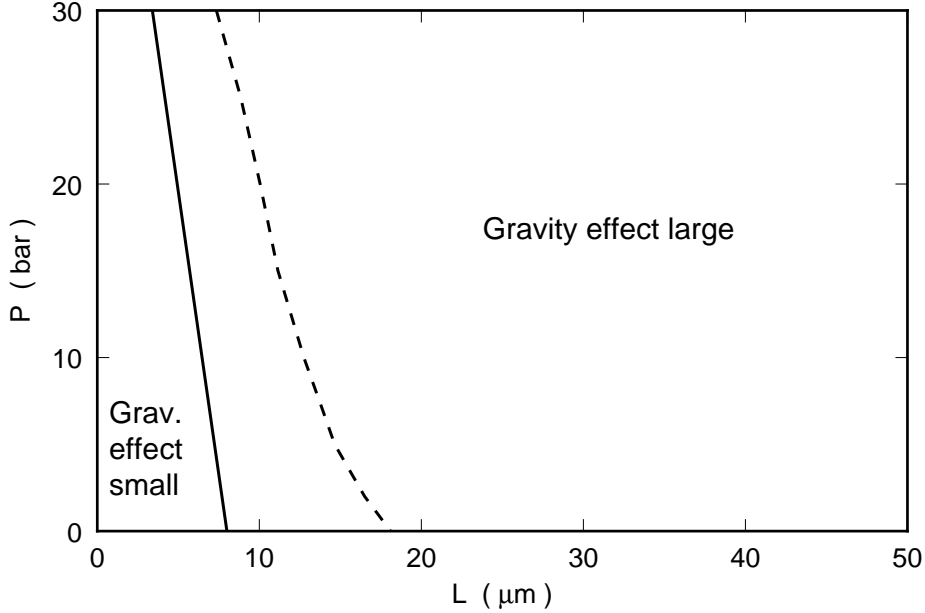


Fig. 22. Summary of the gravity effect as a function of  $P$  and  $L$ . To the left of the line, the gravity effect is relatively small and Earth-based measurements seem feasible. To the right of the line microgravity experiments are necessary.

influence on the experiment. The criterion is naturally somewhat arbitrary. We chose the line where  $\Gamma(L, P)/\Gamma(P)$  reaches 20 % of its value for the bulk system, as indicated by the horizontal dash-dotted line in the Fig. 21 (another choice would merely move the boundary by a small amount). This boundary is shown in Fig. 22 as a dashed line. One can see that by this criterion at SVP the gravity effect becomes important for  $L > 17\mu\text{m}$ , whereas for  $P = 30$  bar it already becomes important near  $L = 7\mu\text{m}$ .

It is interesting to investigate how the gravity effect on  $R$  compares with the effect on other properties such as the heat capacity  $C_P$ . Thus the quantity  $\Gamma_C$  was evaluated in analogy to  $\Gamma$  given by Eq. 21, substituting  $C_{P,g}(t, L)$  and  $C_{P,0}(t, L)$  for  $R_g$  and  $R_0$ . Here  $C_{P,0}(t, L)$  was estimated by scaling the preliminary microgravity results for the parallel-plate geometry from CHeX [9,35] using the scaling function

$$f_C = L^{-\alpha/\nu}[C_{P,0}(t, L) - C_{P,0}(t_0, \infty)] \quad (22)$$

where  $t_0 = (\xi_0/L)^{1/\nu}$ . For  $C_{P,0}(t_0, \infty)$ , the bulk heat capacity given in Ref. [9] was used, as well as it could be determined from the graphs given in that paper (see Ref. [35]). We found that  $\Gamma_C(\infty, P) \simeq 0.062$ , which is a factor of 4.5 smaller than the equivalent result  $\Gamma(\infty, P) \simeq 0.278$  for  $R$ . One sees that the relatively milder singularity in  $C_P$  leads to a smaller gravity effect than for  $R$ . However, the finite-size effects on  $C_P$  are also relatively smaller for  $C_P$ , and thus one would like to have proportionally more quantitative results for

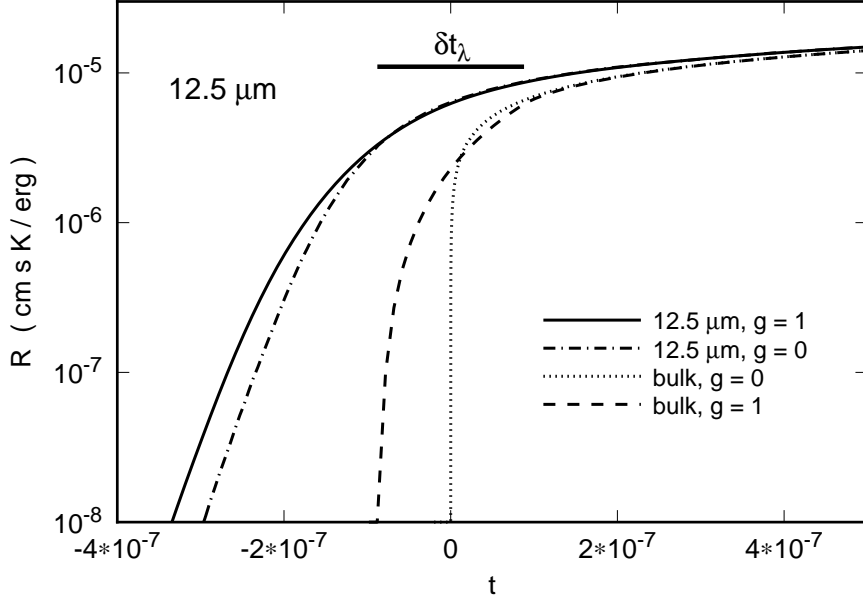


Fig. 23. Estimates of the resistivity for a sample at SVP, of height  $h = 3$  mm, and with  $L = 12.5\mu\text{m}$  as in Fig. 17, but with a logarithmic vertical scale.

$C_P(t, L)$ . Therefore a more appropriate measure of the severity of the gravity effect is again the ratio  $\Gamma_C(L, P)/\Gamma_C(P)$ . For SVP this is shown in Fig. 21 as a dotted line. One sees that by this criterion the gravity effect on  $C_P$  is just as strong as it is for  $R$ .

Closer inspection of the gravity effect reveals that, for  $R$ , the criterion in terms of  $\Gamma$  is somewhat misleading. This is illustrated in Fig. 23, which shows the same data as those of Fig. 17, but with a logarithmic vertical scale. For this example (SVP and  $L = 12.5\mu\text{m}$ )  $\Gamma(L, P)/\Gamma(P) = 0.06$ , which seems to be safely in the range where Earth-based experiments can be corrected for a small gravity effect. However, the figure reveals that the gravity effect is actually overwhelmingly large at low temperatures where the resistivity decays exponentially. The reason for this is of course the exceptionally rapid variation of the exponential function which produces a large effect in the integration over the sample height. For  $t \simeq -3 \times 10^{-7}$ , the ratio  $R_g/R_0$  is approximately equal to three! The gravity effect in this range does not contribute significantly to  $\Gamma$  because  $R$  itself is small. Thus, in order to examine the influence of gravity in the range of the exponential decay of  $R$ , we introduce a different criterion, namely the ratio  $R_g/R_0$  itself. This ratio is shown in Fig. 24 as a function of the reduced temperature. The solid lines are for SVP and the dashed ones pertain to  $P = 30$  bar. Each line is labeled by the value of  $L$  to which it pertains. At its left end each line is terminated when the relevant value of  $R_g$  has decreased to  $10^{-7}$  cm s K / erg, which is about the smallest value at which reliable measurements are feasible in the presence of the boundary resistance. Again we introduce a somewhat arbitrary criterion for dividing the  $L - P$

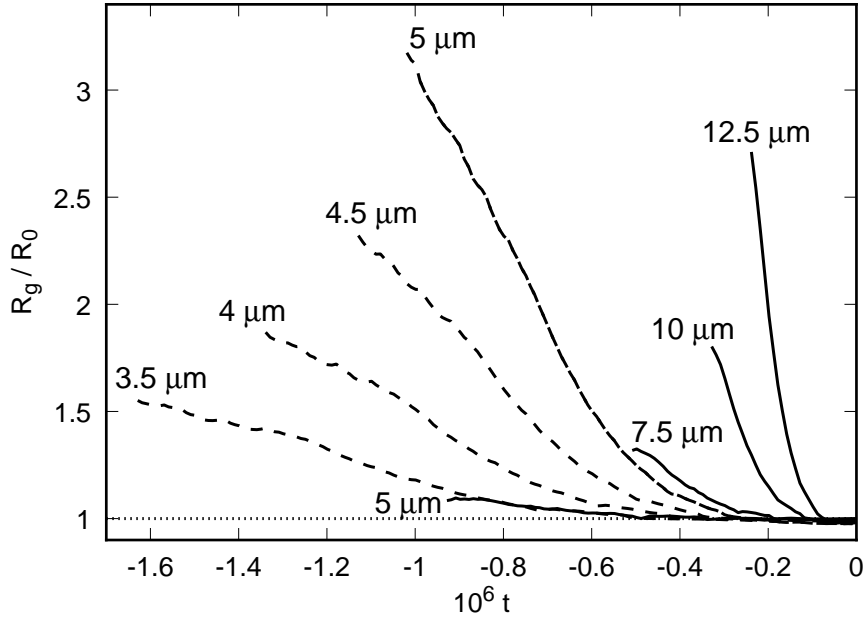


Fig. 24. The ratio  $R_g/R_0$  of the resistivity in the presence of gravity to that for  $g = 0$  as a function of the reduced temperature. The solid lines are for SVP and the dashed ones are for  $P = 30$  bar. The numbers adjacent to the lines give the relevant cylinder radii  $L$ . At their left ends the lines are terminated when  $R_g$  has decreased to  $10^{-7}$  cm s K / erg.

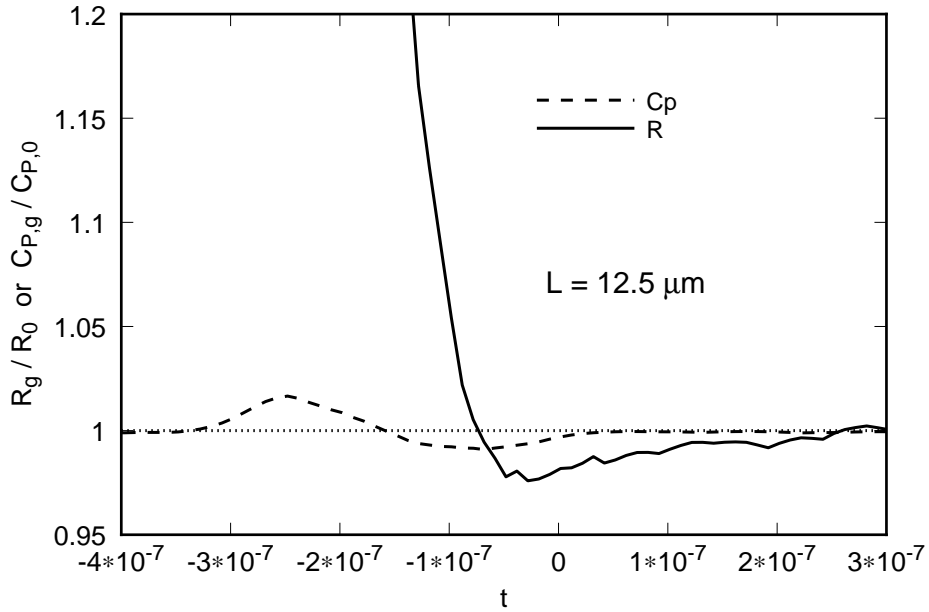


Fig. 25. The ratios  $R_g/R_0$  and  $C_{P,g}/C_{P,0}$  of the resistivity and the heat capacity in the presence of gravity to that for  $g = 0$  as a function of the reduced temperature for  $L = 12.5\mu\text{m}$  at SVP. The solid line is for  $R_g/R_0$  and the dashed one is for  $C_{P,g}/C_{P,0}$ .

plane into two regions by assuming that correction for the gravity effect on Earth can be made reliably when  $R_g/R_0 < 1.5$  in the temperature range where  $R_g > 1 \times 10^{-7}$  cm s K / erg. This criterion yields the solid line in Fig. 22. We see that at SVP gravity becomes of major importance for  $L > 8\mu\text{m}$ . At the highest pressure of 30 bar, this border is located at the rather small value  $L \simeq 3.5\mu\text{m}$ .

Lastly we note that  $C_P$  does not have the extremely rapid (exponential) variation that is seen for the resistivity at low temperatures. Thus in the case of  $C_P$  the parameter  $\Gamma$  defined by Eq. 21 can be used to define an adequate criterion for the importance of gravity, and we expect that the dashed line in Fig. 22 is the appropriate one for  $C_P$  even though an evaluation at elevated pressure has not yet been carried out. A more detailed illustration of the difference between the gravity effect on  $R$  and on  $C_P$  is given in Fig. 25. This illustrative case is for  $h = 3\text{mm}$ , SVP, and  $L = 12.5\mu\text{m}$ . For this case one sees that the gravity effect for  $C_P$  is never larger than about 1.7 %, whereas for  $R$  it grows seemingly without limit as the temperature is reduced. From Fig. 24 we see that for the case illustrated here the ratio for  $R$  reaches a value of about 2.7 before  $R$  has decreased to a size which is comparable to the boundary resistance.

## References

- [1] See, for instance, M.E. Fisher, in *Critical Phenomena*, Proc. 51st “Enrico Fermi” Summer School, Varenna, edited by M. Green (Academic, NY, 1971), p. 1.
- [2] See, for instance, V. Dohm, *Phys. Script.* **T49**, 46 (1993).
- [3] F.M. Gasparini and I. Rhee, in *Prog. Low Temp. Phys.* XIII, edited by D. F. Brewer (North-Holland, Amsterdam, 1992), p. 1.
- [4] T.P. Chen and F.M. Gasparini, *Phys. Rev. Lett.* **40**, 331 (1978).
- [5] F.M. Gasparini, T.P. Chen, and B. Bhattacharyya, *Phys. Rev. B* **23**, 5797 (1981).
- [6] I. Rhee, F.M. Gasparini, and D.J. Bishop, *Phys. Rev. Lett.* **63**, 410 (1989).
- [7] M. Coleman and J. Lipa, *Phys. Rev. Lett.* **74**, 286 (1995).
- [8] S. Mehta and F.M. Gasparini, *Phys. Rev. Lett.* **78**, 2596 (1997).
- [9] J.A. Lipa, D.R. Swanson, J.A. Nissen, P.R. Williamson, K. Geng, D.A. Stricker, T.C.P. Chui, U. Israelsson, and M. Larson, preprint, June 1998.
- [10] However, the singular contribution near  $T_\lambda$  to the boundary resistance between superfluid  $^4\text{He}$  and a solid is closely related. For experimental studies of this effect, see R.V. Duncan, G. Ahlers, and V. Steinberg, *Phys. Rev. Lett.* **58**, 377 (1987); and R.V. Duncan and G. Ahlers, *Phys. Rev. B* **43**, 7707 (1991); and D. Murphy and H. Meyer, *J. Low Temp. Phys.* **105**, 185 (1996); and H. Fu, H. Baddar, K. Kuehn, and G. Ahlers, *Fizika Nizkikh Temperatur* **24**, 101 (1998) [*Low Temp. Phys. (Ukraine)* **24**, 69 (1998)]. Renormalization-group theoretical calculations for this effect have been given by D. Frank and V. Dohm, *Phys. Rev. Lett.* **62**, 1864 (1989); *Z. Phys. B* **84** 443 (1991).
- [11] A. Kahn and G. Ahlers, *Phys. Rev. Lett.* **74**, 944 (1995).
- [12] Glass capillary arrays are available commercially from Galileo Electro-Optics Corporation, Galileo Park, P.O. Box 550, Sturbridge, MA 01566 (1-800-648-1800), and from Collimated Holes, Inc., 460 Division Street, Campbell, CA 95008 (408-374-5080), and from Hamamatsu Corp., 25864 Business Center Drive, Suite A, Redlands, CA 92347 (909-796-6288). Capillary sizes from  $L = 1\mu\text{m}$  to  $50\mu\text{m}$  can be obtained. For the smaller values of  $L$ , the arrays have a thickness of up to 1 mm, whereas for the thicker ones thicknesses up to 5 mm are available. GCAs with  $L < 1\mu\text{m}$  can also be produced; see for instance R.J. Tonucci, B.L. Justus, A.J. Campillo, and C.E. Ford, *Science* **258**, 783 (1992).
- [13] G. Ahlers, *Phys. Rev.* **171**, 275 (1968); *J. Low Temp. Phys.* **84**, 173 (1991).
- [14] G. Ahlers, *Phys. Rev. Lett.* **21**, 1159 (1968).
- [15] J. Kerrisk and W.E. Keller, *Phys. Rev.* **177**, 341 (1969).

- [16] W.Y. Tam and G. Ahlers, Phys. Rev. B **32**, 5932 (1985).
- [17] M. Dingus, F. Zhong, and H. Meyer, J. Low Temp. Phys. **65**, 185 (1986).
- [18] W.Y. Tam and G. Ahlers, Phys. Rev. B **33**, 183 (1986).
- [19] Important early papers include B.I. Halperin, P.C. Hohenberg, and E.D. Siggia, Phys. Rev. Lett. **32**, 1289 (1974); Phys. Rev. B **13**, 1299 (1976); and E.D. Siggia, Phys. Rev. B **13**, 3218 (1976); and C. DeDominici and L. Peliti, Phys. Rev. Lett. **38**, 505 (1977); Phys. Rev. B **18**, 353 (1978); and V. Dohm, Z. Phys. B **31**, 327 (1978); and R.A. Ferrell and J.K. Bhattacharjee, Phys. Rev. Lett. **42**, 1638 (1979); J. Low Temp. Phys. **36**, 165 (1979); and P.C. Hohenberg, B.I. Halperin, and D.R. Nelson, Phys. Rev. B **22**, 2372 (1980); and V. Dohm and R. Folk, Z. Phys. B **40**, 79 (1980); Phys. Rev. Lett. **46**, 349 (1981); and G. Ahlers, P.C. Hohenberg, and A. Kornblit, Phys. Rev. Lett. **36**, 493 (1981); Phys. Rev. B **25**, 3136 (1982); and V. Dohm and R. Folk, Z. Phys. B **45**, 129 (1981); **41**, 251 (1981). The most complete version of the theory was presented by V. Dohm, Phys. Rev. B **44**, 2697 (1991). Detailed tabulations of the parameters which correspond to a fit of this theory to the thermal-conductivity data of Ref. [16] are given by V. Dohm and G. Moser, in Physics Auxiliary Publication Service, Document number PRBMD-44-2697-13.
- [20] L.S. Goldner and G. Ahlers, Phys. Rev. B **45**, 13129 (1992).
- [21] T.C.P. Chui, D.R. Swanson, M.J. Adrians, J.A. Nissen, and J.A. Lipa, in *Temperature: its Measurement and Control in Science and Industry*, Vol. 6, edited by J.F. Schooly (American Institute of Physics, N.Y., 1992).
- [22] A brief report of such measurements at SVP has been published by J. Lipa and Q. Li, Czechoslovak J. Phys. **46**-Suppl, 185 (1996).
- [23] J.A. Lipa and T.C.P. Chui, Phys. Rev. Lett. **58**, 1340 (1987).
- [24] W.Koch, V. Dohm, and D. Stauffer, Phys. Rev. Lett. **77**, 1789 (1996) demonstrated the validity of dynamic finite-size scaling for relaxational dynamics, cubic geometry and periodic boundary conditions, above and below  $T_c$ . Quantitative agreement between theory and Monte Carlo data was obtained by them. W.Koch and V. Dohm, Phys. Rev. E. in print predicted the dynamic finite-size scaling function for the effective diffusion constant of model C of Halperin, Hohenberg, and Siggia [25] (HHS), cubic geometry, periodic boundary conditions, above and below  $T_c$ . J.K. Bhattacharjee, Phys.Rev.Lett. **77**, 1524 (1996) derived an approximate form of the scaling function for the conductivity using a decoupled-mode approximation and Model E of HHS. His result should be qualitatively applicable to the superfluid transition sufficiently far above  $T_\lambda$  and is consistent with a scaling form proposed phenomenologically by KA for that temperature range. To my knowledge no calculations for Model F of HHS with Dirichlet boundary conditions (which would correspond to the superfluid transition of  $^4\text{He}$ ) have been carried out so far.
- [25] B.I. Halperin, P.C. Hohenberg, and E.D. Siggia, in Ref. [19]. See also P.C. Hohenberg and B.I. Halperin, Rev. Mod. Phys. **49**, 435 (1977).

- [26] A. Singaas and G. Ahlers, Phys. Rev. B **30**, 5103 (1984).
- [27] G. Ahlers, Phys. Rev. **135**, A10 (1964).
- [28] H.A. Kierstead, Phys. Rev. **162**, 153 (1967).
- [29] D.S. Greywall and G. Ahlers, Phys. Rev. Lett. **28**, 1251 (1972); Phys. Rev. A **7**, 2145 (1973).
- [30] In Ref. [16] an early estimate of  $\xi_0/\xi_0^T$  from Ref. [31] was used. A re-evaluation on the basis of the most recent information for universal ratios should be carried out. However, the pressure dependence of  $\xi_0$  comes from the pressure dependence of  $\rho_s$  and thus will not be affected. A re-analysis of  $\rho_s$  using the most recent values of the critical exponent  $\nu$  would, however, yield slightly different results for  $\xi_0(P)$ .
- [31] P.C. Hohenberg, A. Aharony, B.I. Halperin, and E.D. Siggia, Phys. Rev. B **13**, 2986 (1976).
- [32] See Table XI of Ref. [16].
- [33] See, for instance, A. Onuki, J. Low Temp. Phys. **104**, 133 (1996).
- [34] See for instance Appendix C of Ref. [16].
- [35] For bulk helium we used the fit to the LPE data [36], with  $\delta C_P = 0.55(1.1)$  J/mole K added below (above)  $T_\lambda$ . The addition of  $\delta C_P$  was necessary to reproduce the dashed curves for bulk helium shown in Fig. 6 of Ref. [9] within our ability to read the graph. These dashed curves were used by Lipa et al., together with the CHeX results, to derive  $f_2$  given in Fig. 7 of Ref. [9], and yield consistency with the theoretically expected scaling function.
- [36] J.A. Lipa, D.R. Swanson, J.A. Nissen, T.C.P. Chui, and U.E. Israelsson, Phys. Rev. Lett. **76**, 944 (1996). The fit parameters are given in footnote 22. There the units of  $A'$  and  $B'$  are J/mole K. In Eq. 1 of this paper,  $A$  should be replaced by  $A/\alpha$ .